RESEARCH ARTICLE

Cr₂O₃ nanoparticles: Synthesis, characterization, optical, magnetic properties and their photocatalytic degradation of methyl orange

Aliakbar Dehno Khalaji*,1, Pavel Machek 2, Marketa Jarosova 2

¹ *Department of Chemistry, Faculty of Science, Golestan University, Gorgan, Iran*

² *Institute of Physic of the Czech Academy of Sciences, Na Slovance 2, Prague, Czech Republic*

ARTICLE INFO

ABSTRACT

Cr_2O_3 nanoparticles are synthesized *via* solid-state thermal decomposition of the mixture of $Cr(NO_3)_3 \cdot 9H_2O$ (as Cr precursor) and benzoic acid (as fuel) at 500 or 600 ºC for 3 h and characterized by FT-IR and UV-Vis spectroscopy, VSM, XRD and TEM. Also, characterized using zeta potential PZ measurement. FT-IR and XRD results confirm high degree of crystallinity of Cr_2O_3 nanoparticles with ≈ 16-18 nm average crystallite size. The size distribution of the as-prepared Cr_2O_3 nanoparticles is estimated to be in the range of 10-60 nm using TEM images. The morphology of the as-prepared Cr_2O_3 nanoparticles is almost ellipsoidal or pseudo-spherical. In addition, the photocatalytic degradation of methyl orange (MO) under UV light was studied. The effects of pH solution, sorbent dose and irradiation time were investigated. Based on changes in the UV-Vis spectra of MO, photocatalytic efficiencies were calculated about 91% and 89% for CeO_2 nanoparticles prepared at 500 or 600 ºC, respectively.

INTRODUCTION

Chromium oxide (its natural form is known as eskolaite) is an important transition metal oxide, that has been in the research spotlight for many years [1-5] and has been widely applied in various fields such as H_2 adsorption [6], catalyst [7], sensing electrodes [8], solar absorbers [9], green pigments [10] and photonic and electronic devices [11,12]. Until now, various methods have been used for the preparation of Cr_2O_3 nanoparticles such as microemulsion [5], sol-gel [13], microwave irradiation [14], hydrothermal [1, 15, 16] and thermal decomposition of various precursors [3, 4, 17-19]. Thermal decomposition is a simple, cheap and fast technique for the preparation of diverse transition metal oxides nanoparticles [17-20]. Recently, Guunewiek [17] synthesized rhombohedral Cr_2O_3 nanoparticles *via* thermal decomposition of a polyacrylate/chromium complex at 480 ºC for 2 h. Sun et al. synthesized

a hollow microsphere of Cr_2O_3 by thermal decomposition of a precursor which was prepared *via* a mild template-free hydrothermal approach at 500 ºC for 4 h [18]. Zhang *et al.* prepared Cr_2O_3 nanoparticles through the thermal decomposition of chromium hydroxide precursor at 950 ºC for 1.5 h [19].

The reduction of environmental pollution caused by different molecules such as phenol [21,22], toluene [23,24], NO_2 [25] and organic dyes [26-32] coming from various industries such as textile, plastic, rubber and dye manufacturing, is one of the biggest challenges in recent years. The dyes can generate toxic and dangerous by-products due to oxidation, hydrolysis and other chemical reactions [26-32]. Methyl orange (MO) is an anionic dye (Scheme 1), widely used in titration as a pH indicator. Recently, photocatalytic degradation of MO has attracted significant attention due to high efficiency, non-toxicity and low cost [31-36].

This paper reports the preparation of new

---

* Corresponding Author Email: *alidkhalaji@yahoo.com*
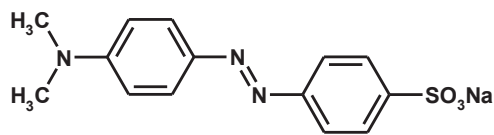
Scheme 1. Chemical structure of methyl orange.

pseudo-spherical Cr$_2$O$_3$ nanoparticles (Cr-1-500 and Cr-1-600) via solid-state thermal decomposition of chromium precursor at two different temperatures (500 ºC and 600 ºC). In addition, the photocatalytic activity of nanoparticles was evaluated through the degradation of MO under UV irradiation. The effects of solution pH, catalyst dose and contact time on the degradation of MO were determined.

EXPERIMENTAL
Materials
All input materials (Cr(NO$_3$)$_2$·9H$_2$O, benzoic acid, methyl orange) are commercially available from Merck Co. and they were used as received without further purifications.

Synthesis of Cr$_2$O$_3$ nanoparticles
1 mmol of Cr(NO$_3$)$_2$·9H$_2$O was dissolved in 5 mL of H$_2$O under vigorous stirring and mixed with a solution of benzoic acid (1 mmol in 5 mL H$_2$O). The mixture was stirred for 0.5 h, transferred into a crucible and maintained at 80 ºC for 3 h to dry completely. After that, the product was annealed at 500ºC or 600 ºC in air atmosphere for 3 h. The green products were rinsed several times with deionized water and ethanol, and finally they were dried overnight at 65 ºC in the oven.

Characterization
FT-IR spectra were recorded using a FT-IR Perkin-Elmer spectrophotometer. UV-Vis spectra were carried out using a Jasco spectrophotometer. The magnetization was recorded by the vibrating sample magnetometer (VSM). XRD patterns were obtained on Empyrean powder diffractometer of PANalytical in the range of $2\theta = 10-80°$ (Cu Kα radiation, $\lambda = 1.5418$ Å). TEM images were recorded on transmission electron microscope Philips CM120. Zeta potential of as-prepared Cr-1-500 and Cr-1-600 nanoparticles were determined with Zetasizer Nano ZS, Malvern Panalytical.

Photocatalytic experiment
The photocatalytic activity of Cr-1-500 and Cr-1-600 nanoparticles was investigated by the degradation of MO under UV irradiation using a 500 W mercury lamp. Typically, various amounts (0.1 and 0.2 g) of Cr-1-500 and Cr-1-600 nanoparticles were added into 50 mL aqueous solution of MO (20 ppm). The suspensions were stirred for 60 min in the dark to achieve an equilibrium sorption/desorption of MO on the surface of Cr-1-500 and Cr-1-600 nanoparticles. Afterwards, the solution was exposed to the UV irradiation. At specific time of irradiation, the nanoparticles were separated in the centrifuge and the residual MO concentration was determined using UV-Vis spectrophotometer at $\lambda_{max} = 464$ nm. [33,35].

RESULTS AND DISCUSSION
Characterization of Cr$_2$O$_3$ nanoparticles
FT-IR spectra
Fig. 1 shows the FT-IR spectra of the as-prepared Cr-1-500 and Cr-1-600 nanoparticles. The peaks below 800 cm^{-1} in the metal oxides are generally caused by inter-atomic vibrations [38]. Likewise two peaks at about 620 and 557 cm^{-1} in Fig.1 are assigned to the Cr-O vibrations in rhombohedral Cr$_2$O$_3$. Broad characteristic bands at about 3418 cm^{-1} for Cr-1-500 and 3403 cm^{-1} for Cr-1-600 are ascribed to the O-H stretching vibration due to the chemisorption of water molecules on the surface of Cr$_2$O$_3$ nanoparticles [37-43]. The weak bands at 1644 cm^{-1} and 1627 cm^{-1} may be well attributed to the stretching of non-dissociated water molecules adsorbed at the surface of Cr-1-500 and Cr-1-600.

UV-Vis spectra
Fig. 2 shows the UV-Vis spectra of the as-prepared Cr-1-500 and Cr-1-600 nanoparticles. The broad absorption peak at about 300 nm can be assigned to the band gap transition of Cr^{4+} ion [38]. Two shoulder peaks, observed at about 480 and 610 nm, are attributed to the d^3 electronic transitions of Cr^{3+} ions, situated in six-coordinate geometry and in octahedral symmetry [41].

VSM
Fig. 3 depicts the magnetization versus applied magnetic field (M-H) curves for the as-prepared Cr-1-500 and Cr-1-600 nanoparticles. The magnetization increases linearly in the region of higher magnetic field and both M-H curves do not reach the saturation. This behavior is usually attributed to the weak ferromagnetism [26]. It might arise from the finite-size effect and modification
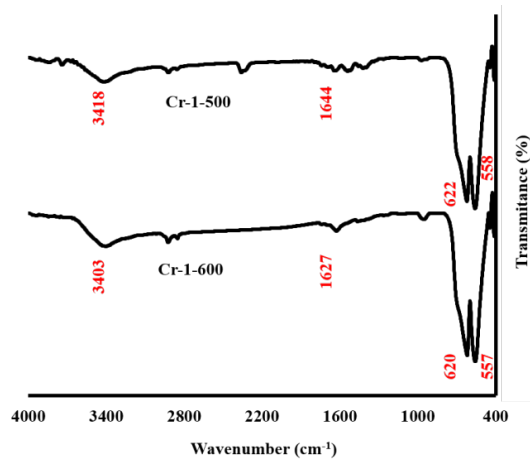
Fig. 1. FT-IR spectra of the as-prepared Cr-1-500 and Cr-1-600 nanoparticles
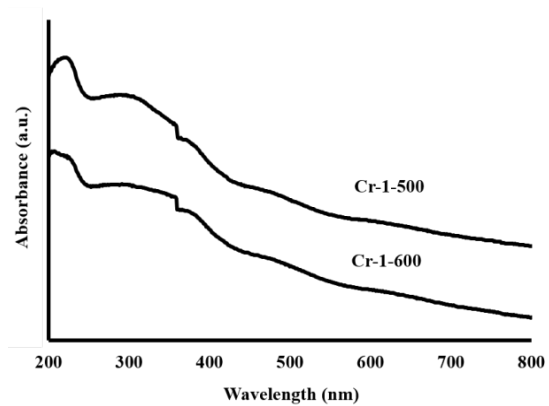
Fig. 2. UV-Vis spectra of the as-prepared Cr-1-500 and Cr-1-600 nanoparticles
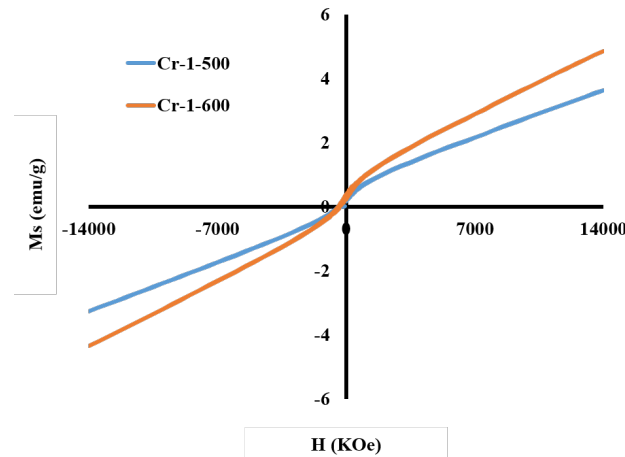
Fig. 3. VSM of the as-prepared Cr-1-500 and Cr-1-600 nanoparticles

of the bulk state due to surface effects [44, 45]. It suggests that the long-range antiferromagnetic order is destroyed in the nanoscale materials. A small difference between M-H curves of Cr-1-500 and Cr-1-600 indicates differences in the crystallite sizes [12].

XRD Patterns

Fig. 4 reveals XRD patterns of both as-prepared samples. Observed diffraction peaks are clear and sharp and can be fully assigned to the rhombohedral phase of Cr_2O_3 (JCPDS file no. 38-1479) [14-17]. Rietveld fit confirmed space group 'R-3c' and lattice constants a=4.954(1) Å and c=13.585(5) Å for Cr-1-500 and a=4.9576(3) Å and c=13.597(1) Å for Cr-1-600. The average size of crystallites was calculated from Williamson-Hall plot (Fig. 5) drawn in accordance with the following equation:

$$\beta \cos\theta = \frac{k\lambda}{D} + 4\varepsilon \sin\theta \qquad (1)$$

Where β is FWHM in radians, θ is Braggs angle, λ is wavelength, D is the average crystallite size, e is micro strain and k is a constant between 0.9-1. The average crystallite size determined for Cr-1-500 sample is 15.8 nm and 17.6 nm for Cr-1-600 sample.

TEM images

The morphology and size of the as-prepared Cr-1-500 and Cr-1-600 nanoparticles were characterized by TEM, as shown in Fig. 6. The Cr-1-500 matter predominantly contains single oval-shaped nanoparticles while nanoparticles Cr-1-600 appear to be more spherical. The
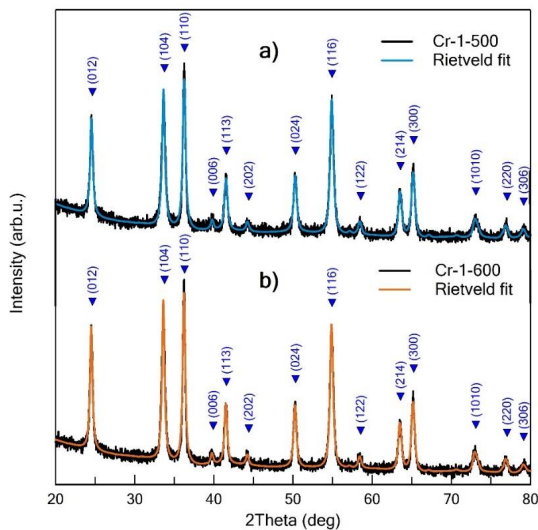
Fig. 4. XRD patterns of the as-prepared Cr-1-500 and Cr-1-600 nanoparticles
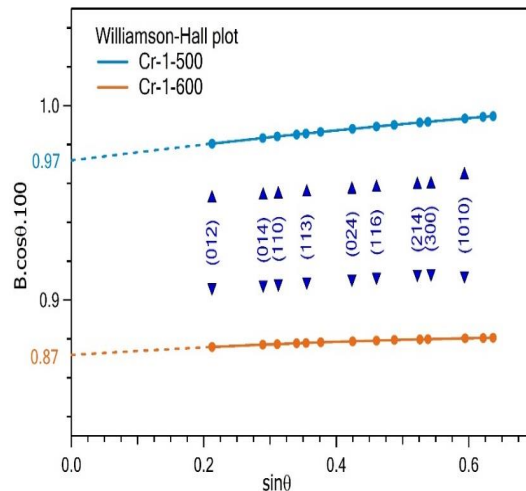
Fig. 5. WH plots of the as-prepared Cr-1-500 and Cr-1-600 nanoparticles
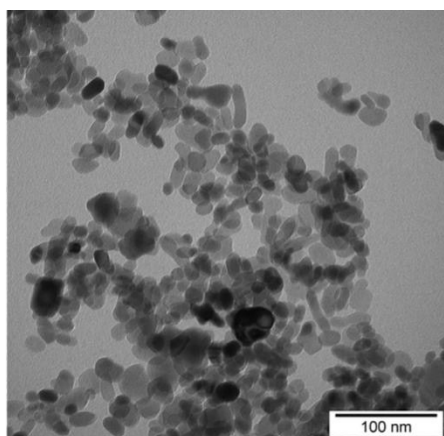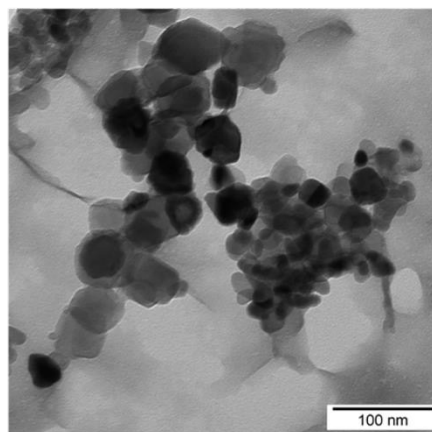
Cr-1-500   Cr-1-600

Fig. 6. TEM images of the as-prepared Cr-1-500 and Cr-1-600 nanoparticles

sizes of the as-prepared Cr-1-500 and Cr-1-600 nanoparticles were observed in the range of 10-60 nm.

Photocatalytic activity

The photocatalytic properties of the as-prepared Cr-1-500 and Cr-1-600 nanoparticles were investigated using MO degradation under UV light irradiation. The degradation of MO is greatly affected by the solution pH because of catalyst aggregation, dye and also the surface charge of catalyst depends on the pH [46]. To determine the surface charge of the as-prepared Cr-1-500 and Cr-1-600 nanoparticles, the Zeta potential was measured at different solution pH and its

values are depicted in Fig. 7. As seen in this figure, nanoparticles Cr-1-500 and Cr-1-600 have point of zero charge (pH$_{PZC}$) at 7.41 and 7.51, respectively. The optimum pH for high adsorption and efficient photodegradation of MO was selected at level 7. At this pH, the positive surface charge of the as-prepared Cr-1-500 and Cr-1-600 nanoparticles can well interact with negative charge of MO by using a strong electrostatic attraction.

The degradation percentage of MO was evaluated by the following equation:

$$D\,(\%) = 100 \times \left(\frac{Co - Ct}{Co}\right) \qquad (2)$$
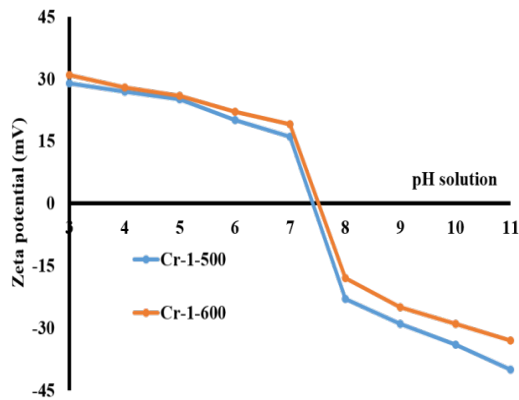
Fig. 7. Zeta potential of the as-prepared Cr-1-500 and Cr-1-600 nanoparticles as function of pH.
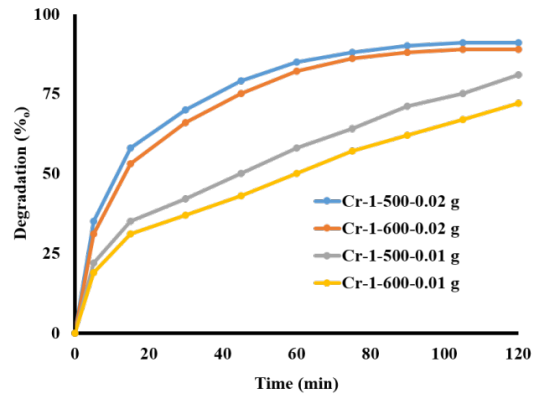
Fig. 8. Effect of catalyst dose and irradiation time on degradation of MO
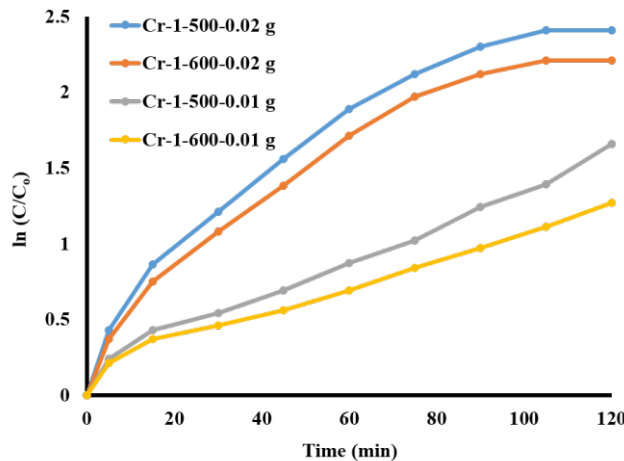
Fig. 9. Langmuir plot of photocatalytic reaction of MO using various amounts of as-prepared Cr$_2$O$_3$ nanoparticles.

Where C$_o$ is the initial concentration of MO (ppm) and C$_t$ is the concentration at irradiation time t. The dependency of MO degradation percentage (%) versus irradiation time is depicted in Fig. 8. The MO degradation increases with increasing irradiation time and reaches its maximum at 91% in the presence of 0.02 g of Cr-1-500 and at 89% in the presence of 0.02 g of Cr-1-600. As seen in Fig. 8, the adsorption amount increases very fast in the first 15 min. The equilibrium is approached after 60 min, when 0.02 g of catalyst used. The photodegradation of MO at equilibrium increases from about 50 to 80% when catalyst dose increases from 0.01 to 0.02 g, due to increases of active sites on the surface of the catalyst.

The kinetics of MO degradation was studied using Langmuir model utilizing following equation:

$$\ln \frac{Ct}{Co} = kt \tag{3}$$

Where k is the reaction rate constant (min^{-1}) and t is irradiation time (min).

The curves of ln $\frac{Ct}{Co}$ versus t are plotted in Fig. 9 for distinct amounts of the as-prepared Cr$_2$O$_3$ nanoparticles. The photocatalytic degradation of MO was found to be of pseudo-first order with rate constants of (k) 1.38×10^{-2}, 1.06×10^{-2}, 2.29×10^{-2} and 2.11×10^{-2} min^{-1} for Cr-1-500-0.01 g, Cr-1-600-0.01 g, Cr-1-500-0.02 g and Cr-1-600-0.02 g, respectively.

The maximum reaction rate was achieved with 0.02 g of Cr-1-500 nanoparticles. The values of k, t and degradation (%) were compared with other catalysts employed for photocatalytic removal of MO and summarized in Table 1.

Table 1. The *k* values of various catalysts used for removal of MO

Catalyst	k (min^{-1})	Degradation (%)	Time (min)	Reference
Ag/TiO$_2$/biochar	6.29×10^{-2}	97.48	60	35
TiO$_2$/ZnO		97.00	30	34
FemIL@SiO$_2$@Mag	6.66×10^{-3}	99.00	30	33
MoS$_2$/Fe$_3$O$_4$	--------	79.53	100	47
Fe$_3$O$_4$@C@Cu$_2$O	--------	100.00	120	48
Fe$_3$O$_4$/ TiO$_2$ (P$_{25}$)	--------	90.30	60	49
Spherical Cr$_2$O$_3$	2.29×10^{-2}	91.00	105	this work

CONCLUSIONS

In summary, Cr$_2$O$_3$ nanoparticles with pseudo-spherical shape were prepared by the cheap, simple and eco-friendly method and the basic characterizations were performed. According to the XRD, the average crystallite size of Cr$_2$O$_3$ nanoparticles is 15.8 and 17.6 nm. VSM results confirm the weak ferromagnetic behavior of the as-prepared Cr$_2$O$_3$ nanoparticles. The photocatalytic degradation results indicate that the maximum of MO removal is 91% and was achieved after 105 min UV irradiation of 0.02 g dose of Cr-1-500 nanoparticles with reaction rate constant of $k = 2.29\times10^{-2}$ min^{-1}. The photodegradation of MO increases when the catalyst dose is increased from 0.01 to 0.02 g, because active sites are raised on the surface of catalyst.

It is proved in the paper, that the method is suitable for the synthesis of Cr$_2$O$_3$ nanoparticles. We propose to use this method in a similar way for the preparation of other transition metal oxide nanoparticles such as CuO and Fe$_2$O$_3$.

ACKNOWLEDGMENTS

CONFLICT OF INTEREST

The authors declare no conflicts of interest.

REFERENCES

[1] Z. Pei, Y. Zhang, Mater. Lett. 62 (2008) 504. https://doi.org/10.1016/j.matlet.2007.05.073

[2] M.W. Abee, S.C. York, D.F. Cox, J. Phys. Chem. B 105 (2001) 7755. https://doi.org/10.1021/jp011223u

[3] L. Li, Z.F. Yan, G.Q. Lu, Z.H. Zhu, J. Phys. Chem. B 110 (2006) 178. https://doi.org/10.1021/jp053810b

[4] B.A. Kalantari, M.R. Talei Bavil Olyai, J. App. Chem. Res. 47 (2015) 47.

[5] R. Karimian, F. Piri, J. Nanostruct. 3 (2013) 87. https://doi.org/10.1186/2193-8865-3-52

[6] J.L. Bobet, S. Desmoulins-Krawiec, E. Grigorova, F. Cansell, B. Chevalier, J. All. Compd. 351 (2003) 217. https://doi.org/10.1016/S0925-8388(02)01030-7

[7] J.H. Uhm, M.Y. Shin, Z.D. Jiang, J.S. Chung, Appl. Catal. B 22 (1999) 293. https://doi.org/10.1016/S0926-3373(99)00057-0

[8] H. Zhang, J.G. Li, H.B. Zhang, X.S. Liang, C.G. Yin, Q. Diao, J. Zhrng, G.Y. Lu, Sensor Actuat. B. Chem. 180 (2013) 66. https://doi.org/10.1016/j.snb.2012.03.024

[9] S, Khamlich, O. Nemraoui, N. Mongwaketsi, R. McCrindle, N. Cingo, M. Maaza, Physica B 407 (2012) 1509. https://doi.org/10.1016/j.physb.2011.09.073

[10] P.M.T. Cavalcante, M. Dondi, G. Guarini, M. Raimondo, G. Baldi, Dyes Pig. 80 (2009) 226. https://doi.org/10.1016/j.dyepig.2008.07.004

[11] X. He, D. Antonelli, Angew. Chem. Int. Ed. 114 (2002) 222. https://doi.org/10.1002/1521-3757(20020118)114:2<222::AID-ANGE222>3.0.CO;2-5

[12] X. He, D. Antonelli, Angew. Chem. Int. Ed. Engl. 41 (2002) 214. https://doi.org/10.1002/1521-3773(20020118)41:2<214::AID-ANIE214>3.0.CO;2-D

[13] V. Balouria, A. Singh, A.K. Debnath, A. Mahajan, R.K. Bedi, D.K. Aswal, S.K. Gupta, Solid State Phys. AIP Conf. Proc. 1447 (2012) 341.

[14] F. Farzaneh, M. Najafi, J. Sci. IRI. 22 (2011) 329.

[15] Z. Pei, X. Zhang, Mater. Lett. 93 (2013) 377. https://doi.org/10.1016/j.matlet.2012.11.127

[16] Z. Pei, J. Pei, H. Chen, L. Gao, S. Zhou, Mater. Lett. 159 (2015) 357. https://doi.org/10.1016/j.matlet.2015.07.012

[17] R.F.K. Gunnewiek, C.F. Mendes, R.H.G.A. Kiminami, Mater. Lett. 129 (2014) 54. https://doi.org/10.1016/j.matlet.2014.05.026

[18] H. Sun, L. Wang, D. Chu, Z. Ma, A. Wang, Mater. Lett. 140 (2015) 35.

[19] H.L. Zhang, S.T. Liang, M.T. Luo, M.G. Ma, P.P. Fan, H.B. Xu, P. Li, Y. Zhang, Mater. Lett. 117 (2014) 244. https://doi.org/10.1016/j.matlet.2013.12.010

[20] N.D. Hebbar, K.S. Choudhari, S.A. Shivashankar, C. Santhosh, S.D. Kulkarni, J. Alloys Compd. 785 (2019) 747.

https://doi.org/10.1016/j.jallcom.2019.01.254

[21] A. Shokri, Int. J. Environ. Anal. Chem. doi.10.1080/03067 319.2020.1791328

[22] A. Shokri. Russ. J. Phys. Chem. A 93 (2019) 243. https://doi.org/10.1134/S003602441902002X

[23] A. Shokri, Int. J. Environ. Anal. Chem. doi.10.1080/03067 319.2020.1784887

[24] M. Rostami, H. Mazaheri, A. Hassani Joshaghani, A. Shokri, Int. J. Eng. B 32 (2019) 1074.

[25] A. Shokri, Surf. Interfaces. 21 (2020) 100705. https://doi.org/10.1016/j.surfin.2020.100705

[26] A.D. Khalaji, P. Machek, M. Jarosova, Adv. J. Chem. A 4 (2021) 317.

[27] A. Foroughnia, A.D. Khalaji, E. Kolvari, N. Koukabi, Int. J. Biol. Macromol. 177 (2021) 83. https://doi.org/10.1016/j.ijbiomac.2021.02.068

[28] Z. Bashandeh, A.D. Khalaji, Asian J. Nanosci. Mater. 4 (2021) 274.

[29] M. Sanati, A.D. Khalaji, A. Mokhtari, M. Keyvanfard, Prog. Chem. Biochem. Res. 4 (2021) 319.

[30] Z. Bashandeh, A.D. Khalaji, Adv. J. Chem. A 4 (2021) 270.

[31] S. Steplin Paul Selvin, A. Ganesh Kumar, L. Sarala, R. Rajaram, A. Sathiyan, J. Princy Merlin, I. Sharmila Lydia, ACS Sustainable Chem. Eng. 6 (2018) 258. https://doi.org/10.1021/acssuschemeng.7b02335

[32] M.A. Iqbal, S.I. Ali, F. Amin, A. Tariq, M.Z. Iqbal, S. Rizwan, ACS Omega 4 (2019) 8661. https://doi.org/10.1021/acsomega.9b00493

[33] A.G. Naikwade, M.B. Jagadale, D.P. Kale, A.D. Gophane, K.M. Garadkar, G.S. Rashinkar, ACS Omega 5 (2020) 131. https://doi.org/10.1021/acsomega.9b02040

[34] R. Zha, R. Nadimicherla, X. Guo, J. Mater. Chem. A 3 (2015) 6565.

[35] R. Shan, L. Lu, J. Gu, Y. Zhang, H. Yuan, Y. Chen, B. Luo, Mater. Sci. Semiconduc. Process. 114 (2020) 105088. https://doi.org/10.1016/j.mssp.2020.105088

[36] Y. Bian, G. Zhang, W. Ding, L. Hu, Z. Sheng, RSC Adv. 11 (2021) 6284.

[37] A. Hassan, A. Osman said, B. Heakal, A. Younis, M. Abdelmoaz, M. Abdrabou, Adv. J. Chem. A. 3 (2020) 621.

[38] K. Anandan, V. Rajendran, Mater. Sci. Semiconduc. Process. 19 (2014) 136. https://doi.org/10.1016/j.mssp.2013.12.004

[39] M. Salehi, F. Ghasemi, J. App. Chem. 9 (2015) 97.

[40] B.T. Sone, E. Manikandan, A. Gurib-Fakim, M. Maaza, Gren Chem. Lett. Rev. 9 (2016) 85. https://doi.org/10.1080/17518253.2016.1151083

[41] M. Roy, S. Ghosh, M.K. Naskar, Mater. Chem. Phys. 159 (2015) 101. https://doi.org/10.1016/j.matchemphys.2015.03.058

[42] V. Petricek, M. Dusek, L. Palatinus L. Z. Kristallogr. 229 (2014) 345. https://doi.org/10.1515/zkri-2014-1737

[43] R.W. Cheary, A.A. Coelho, J. Appl. Cryst. 31 (1998) 862. https://doi.org/10.1107/S0021889898006876 https://doi.org/10.1107/S0021889898006888

[44] D.W. Kim, S.I. Shin, J.D. Lee, S.G. Oh, Matter. Lett. 58 (2004) 1894. https://doi.org/10.1016/j.matlet.2003.11.023

[45] A. Sobhani, M.S. Niasari, Superlattices Microstruct. 59 (2013) 1. https://doi.org/10.1016/j.spmi.2013.03.018

[46] M. Lu, Y. Cui, Z. Zhao, A. Fakhri, J. Photochem. Photobiol. B: Biol. 205 (2020) 111842. https://doi.org/10.1016/j.jphotobiol.2020.111842

[47] X. Lin, X. Wang, Q. Zhou, C. Wen, S. Su, J. Xiang, P. Cheng, X. Hu, Y. Li, X. Wang, X. Gao, R. Nozel, G. Zhou, Z. Zhang, J. Liu, ACS Sustainable Chem. Eng. 7 (2018) 1673. https://doi.org/10.1021/acssuschemeng.8b05440

[48] S.K. Li, F.Z. Huang, Y. Wang, Y.H. Shen, L.G. Qiu, A.J. Xie, S.J. Xu, J. Mater. Chem. 21 (2011) 7459. https://doi.org/10.1039/c0jm04569a

[49] N.I.M. Razip, K.M. Lee, C.W. Lai, B.H. Ong, Mater. Res. Express (2019) DOI:10.1088/2053-1591/AB176E https://doi.org/10.1088/2053-1591/ab176e